DOI:
10.1039/C9TB00937J

Document Version
Peer reviewed version

Journal Name

ARTICLE

Low molecular weight PEG-PLGA polymers provide a superior matrix for conjugated polymer nanoparticles in terms of physicochemical properties, biocompatibility and optical/photoacoustic performance

Received 00th January 20xx,
Accepted 00th January 20xx

DOI: 10.1039/x0xx00000x

www.rsc.org/

Thais Fedatto Abelha[a]*, Paul Robert Neumann[b]*, Joost Holthof[c], Cécile A. Dreiss[d], Cameron Alexander[a], Mark Green[e] and Lea Ann Dailey[b]

The near-infrared absorbing conjugated polymer poly[2,6-(4,4-bis-(2-ethylhexyl)-4H-cyclopenta[2,1-b;3,4-b']-dithiophene)-alt-4,7-(2,1,3-benzothiadiazole)] (PCPDTBT) has been investigated as a contrast agent for optical and photoacoustic imaging. Lipophilic π-conjugated polymers can be efficiently encapsulated within self-assembling diblock copolymer poly (ethylene glycol) methyl ether-block-poly (lactide-co-glycolide) (PEG-PLGA) nanoparticles, although the effect of variations in PEG and PLGA chain lengths on nanoparticle properties, performance and biocompatbility have not yet been investigated. In this study, PEG-PLGA with different block lengths (PEG_{2kDa}-$PLGA_{4kDa}$, PEG_{2kDa}-$PLGA_{15kDa}$ and PEG_{5kDa}-$PLGA_{55kDa}$) were used to encapsulate PCPDTBT. Nanoparticle sizes were smallest (<100 nm) when using PEG_{2kDa}-$PLGA_{4kDa}$,with < 5% PCPDTBT content and a reduction in the total solids concentration of the organic phase. All PEG-PLGA nanoparticles were colloidally stable in water and serum-supplemented cell culture medium over 24 h at 37°C, with slight evidence of protein surface adsorption. PEG_{2kDa}-$PLGA_{4kDa}$ systems showed a threefold lower cytotoxicity (IC_{50} value) than the other two systems. Haemolytic activity was < 2.5% for all systems and no platelet aggregation or inhibition of ADP-induced platelet aggregation was observed. Encapsulation of PCPDTBT within a PEG-PGLA matrix shifted fluorescence emission towards red wavelengths (760 nm in THF vs 840 nm in nanoparticles) and reduced the quantum yield by 30-70-fold compared to THF. Nonetheless, PCPDTBT: PEG_{2kDa}-$PLGA_{4kDa}$ systems had a marginally higher quantum yield and signal-to-background ratio in a phantom mouse compared with PEG_{2kDa}-$PLGA_{15kDa}$ and PEG_{5kDa}-$PLGA_{55kDa}$ systems. As a photoacoustic imaging probe, PCPDTBT: PEG_{2kDa}-$PLGA_{4kDa}$ systems also showed a higher photoacoustic amplitude compared to higher molecular weight PEG-PLGA systems. Overall, the low molecular weight PEG_{2kDa}-$PLGA_{4kDa}$ nanoparticle systems conferred the benefits of smaller sizes, reduced cytotoxicity and enhanced imaging performance compared to higher molecular weight matrix polymers.

Introduction

Bioimaging is used in research to understand physiological and pathological processes and it plays a crucial role in the diagnosis and monitoring of the progress of disease [1]. Given its importance, there is an increasing demand for biocompatible imaging agents with improved performance that would benefit researchers, patients and medical doctors. Among the different materials explored for the acquisition of images, conjugated polymer nanoparticles (CPNs) are attractive candidates for cellular labelling or biomedical imaging and have emerged as an alternative to quantum dots and small molecule dyes, because they show higher brightness, increased photostability and negligible cytotoxicity [2,3].

The conjugated polymer, poly[2,6-(4,4-bis-(2-ethylhexyl)-4H-cyclopenta[2,1-b;3,4-b']-dithiophene)-alt-4,7-(2,1,3-benzothiadiazole)] (PCPDTBT, **Figure 1**), was first synthesised in 2006 as a promising new low-bandgap material (i.e. requiring a lower amount of energy absorption to conduct [4]) for organic photovoltaic applications [5]. PCPDTBT is composed of alternating units of electron-rich cyclopentadithiophene (CPDT) and electron-poor benzothiadiazole (BT), showing maximum absorbance and emission in the near infra-red [5,6] (**Figure 1**). While the broad absorbance of PCPDTBT within the terrestrial solar spectrum has attracted attention for improved performance of organic solar cells [6–9], its near-infrared absorbance/emission and photoacoustic properties is promising for biomedical imaging applications [10–15] and photothermal ablation [11,12,16–18].

[a] School of Pharmacy, University of Nottingham, University Park, Nottingham NG7 2RD, UK.
[b] Institute of Pharmacy, Martin-Luther-Universität Halle-Wittenberg, Halle, Germany.
[c] FUJIFILM Visualsonics, Joop Geesinkweg 140, 1114 AB, Amsterdam, The Netherlands
[d] King's College London, School of Cancer & Pharmaceutical Sciences, Waterloo Campus, SE1 9NH, London, UK.
[e] King's College London, Department of Physics, Strand Campus, WC2R 2LS, London, UK. Email: mark.a.green@kcl.ac.uk
Correspondence: Email: lea.dailey@pharmazie.uni-halle.de
*These authors have contributed equally.

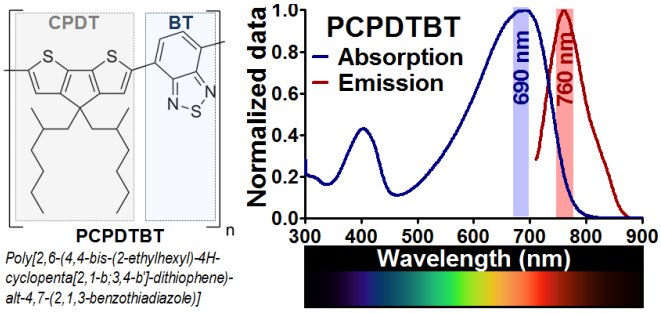

Figure 1: Chemical structure, absorption and emission spectra of PCPDTBT in tetrahydrofuran (THF).

As a highly lipophilic polymer, PCPDTBT is typically embedded in nanoparticle-based structures with varying chemical composition and characteristics [6–14]. Several studies report using nanoprecipitation or mini-emulsion methods to produce CPNs with a PCPDTBT core covered by an adsorbed layer of phospholipid surfactants [10,12,16,19,20], such as 1,2-dipalmitoyl-*sn*-glycero-3-phosphocholine (DPPC) [10,20]. Triblock copolymers of PEG and poly-(propylene glycol) (PEG-*b*-PPG-*b*-PEG) have also been used [11], as well as strategies that embed the conjugated polymer within silica creating multi-layer nanoparticle architectures [13,14,21]. The disadvantage of core-shell CPNs is the observation that many types of amphiphilic stabilising agents, such as phospholipids, are displaced from the particle surface in biological fluids [22]. Nonetheless, PCPDTBT/DPPC CPNs have shown strong and stable photoacoustic (PA) signals, enabling whole-body lymph-node mapping in living mice at low mass concentration[10], while PA imaging and photothermal ablation of tumours in living mice was achieved with nanoparticles of PCPDTBT doped with (6,6)-phenyl-C71-butyric acid methyl ester (PC70BM) prepared with PEG-*b*-PPG-*b*-PEG [11].

The biodegradable copolymer, poly (ethylene glycol) methyl ether-block-poly (lactide-co-glycolide) (PEG-PLGA), has been extensively investigated for drug delivery applications due to its excellent degradation and biocompatibility [23,24]. Additionally, PEG-PLGA has been successfully used as a encapsulating agent for conjugated polymers [25,26]. The lipophilic PLGA chains self-assemble in aqueous solutions to form a hydrophobic matrix which can effectively incorporate lipophilic compounds, whilst the PEG component of the diblock copolymer provides steric stabilisation through orientation of the hydrophilic PEG chains on the surface of the nanoparticles. This stable PEG coating improves colloidal stability and reduces interactions with blood components, an effect referred to as a stealth behaviour [27]. Due to the self-assembling characteristics of the amphiphilic PEG-PLGA copolymer, nanoparticles can be prepared through nanoprecipitation, a simple and low energy input process with a high product yield [28,29].

Nanoparticles engineered for biomedical imaging applications should perform their designated function without harming tissues and cells that are exposed to them [30,31]. A pre-clinical evaluation of nanoparticle interactions with cells is usually the first step to evaluate the risk-benefit ratio of a new material [30]. Preliminary biocompatibility assays include the *in vitro* examination of the interaction of nanoparticles with relevant biological components such as those present in blood [30,31]. While many reports of CPNs prepared for bioimaging applications have included cytotoxicity assessment in different cell lines [14,17,20–22,26,32], the study of the compatibility of CPNs with relevant blood components is less common in the literature [33]. Additionally, many studies that have shown the potential of CPNs as bioimaging agents did not include any biocompatibility assessment [34–39]. While the physicochemical characterisation of CPNs is vital to rationalise the design of imaging agents, a preliminary safety assessment is a key step towards their commercial and clinical applicability.

In this work, PEG-PLGA of different block lengths (PEG_{2kDa}-$PLGA_{4kDa}$, PEG_{2kDa}-$PLGA_{15kDa}$ and PEG_{5kDa}-$PLGA_{55kDa}$) were investigated as nanocarriers of PCPDTBT. The impact of the different PEG-PLGA compositions on nanoparticle physicochemical properties, biocompatibility and imaging performance was investigated. It was hypothesised that increasing PLGA molecular weight in the diblock copolymer may lead to an increase in nanoparticle size but could also concurrently show a favourable effect on PCPDTBT optical properties, due to an increase in the hydrophobic environment of the embedded conjugated polymer. It was further hypothesised that the embedded PCPDTBT would not influence nanoparticle biocompatibility.

Experimental

Materials

PCPDTBT (cat # 754005) with an average molecular weight of 7482 Da and the three different types of PEG-PLGA copolymers with 50:50 ratio of lactide/glycolide (PEG_{2kDa}-$PLGA_{4kDa}$, PEG_{2kDa}-$PLGA_{15kDa}$ and PEG_{5kDa}-$PLGA_{55kDa}$) were purchased from Sigma-Aldrich Corporation (St Louis, MO, USA), in addition to the following reagents: THF (ReagentPlus®, ≥99.0%,); heat inactivated FBS; purified HPLC water (impurities ≤1ppb and anions ≤ 0.1 mg/kg); NaCl, MTT (3-(4,5-dimethylthazol-2-yl)-2,5-diphenyl tetrazolium bromide), haemoglobin standard (human), Dulbecco's phosphate buffered saline Ca^{2+}/Mg^{2+} free (DPBS), cyanmethemoglobin (CMH) reagent (Drabkin's reagent), adenosine 5'-diphosphate sodium salt (ADP), Triton® X-100 (4-(1,1,3,3-Tetramethylbutyl) phenyl-polyethylene glycol, t-octylphenoxypolyethoxyethanol, polyethylene glycol tert-octylphenyl ether) and trypan blue solution. High glucose phenol red free DMEM cell culture medium (CCM); pen strep (10,000 units of penicillin and 10 mg streptomycin/mL); L-glutamine 200 mM; HEPES buffer 1M and pyruvate 100 mM were obtained from Gibco® (Life Technologies™, Paisley, UK). Dimethyl formamide (DMF, 50% solution) was acquired from Severn Biotech Ltd (Kidderminster, UK). Phosphate buffered saline (PBS) ("Dulbecco A" tablets) was acquired from Oxoid Ltd (England). The BALB/C monocyte-macrophage J774A.1 cell line (TIB-67TM, LOT:60880169) was

acquired from American Type Culture Collection (ATCC®, Virginia, USA). Chemicals were used as received without further purification.

Preparation of nanoparticles

PCPDTBT CPNs were prepared by nanoprecipitation [25,26]. Briefly, 1 mL of PCPDTBT + PEG-PLGA solution in THF was added dropwise to 5 mL of water at room temperature stirred for up to 12 hours to allow complete evaporation of the solvent. The volume of water lost due to evaporation was replaced. Corresponding formulations containing 100% PEG-PLGA were prepared as controls. At least three independent replicate batches of each formulation were produced and characterised. All nanoparticle batches were characterized without filtration or purification. An optimisation study was performed with the three PEG-PLGA structures to assess the effect of PCPDTBT content (0-50% w/w) and total solids concentration (0.2-2.1 mg/mL) on CPN properties.

Dynamic light scattering (DLS) and zeta potential: Hydrodynamic diameters (HD) were assessed by DLS using a Zetasizer NanoZS (Malvern Instruments Ltd, UK) equipped with a 633 nm He-Ne laser and a backscatter detector with a measurement angle of 173°. The size analysis was performed at 25°C (0.8872 cP) at 50 µg/mL total solids concentration. The Z-average value obtained from the intensity distribution of particles size was expressed as a mean diameter for distributions which were found to be monomodal. The zeta potential was measured at 25°C after sample dilution in NaCl 10 mM [40,41] to a final polymer concentration of 20 µg/mL in standard electrophoresis cuvettes (DTS1070, Malvern Instruments GmbH) in a Zetasizer NanoZS (Malvern Instruments Ltd, UK).

Scanning electron microscopy (SEM): Nanoparticles comprised of PEG_{2kDa}-$PLGA_{15kDa}$ or PEG_{5kDa}-$PLGA_{55kDa}$ containing 0 or 5% PCPDTBT (2.1 or 2.0 mg/mL total solids concentration) were assessed by SEM on a Hitachi S-4000 (Tokyo, Japan) at 25 kV and at 0/45°-tilt by air drying 50 µL of nanoparticle solution on a cover slip followed by coating with 15 nm of gold. From SEM images, the nanoparticle size distribution was determined using ImageJ software [42].

Nanoparticle stability in physiological media

The pH, size, and zeta potential of containing 0 or 5% PCPDTBT prepared at 2.1 mg/mL total solids concentration was measured before and after 24-hour incubation period at 37°C in water and CCM (DMEM supplemented with 10% FBS, 1% antibiotics, 1% L-glutamine 200mM, 1% HEPES buffer 1M and 1% pyruvate 100 mM) at final nanoparticle concentration of 300 µg/mL. Nanoparticle tracking analysis (NTA; Malvern Instruments Ltd, UK) was used to assess hydrodynamic diameter in this study component. Following incubation, the formulations were diluted to 10.5 µg/ml with filtered (0.22 µm CA filter) bidistilled water before NTA measurement (532nm laser unit). Data is shown in Figure S1, ESI.

MTT cytotoxicity assay: The J774A.1 cell line (referred to J77A for simplicity) was mycoplasma free, tested by the Hoechst stain (Bisbenzimide H 33258) method [43]. J774 cells were cultured in DMEM supplemented with 10% FBS, 1% antibiotics (100 U penicillin and 0.1 mg/ml streptomycin), 1% sodium pyruvate (100 mM) and 5% L-glutamine (200 mM). For the MTT assay, 60 inner wells of a 96-well plate were seeded with 25,000 cells/well [44] and the tetrazolium salt MTT colorimetric assay was used to assess the J774 cell line survival following incubation at 37°C for 24 h with nanoparticle suspensions (200 µL; nanoparticle concentration 0.1-300 µg/mL) in CCM. To control for effects of hypotonicity, CCM was diluted in the following ratios 1:4, 1:12 and 1:32 H_2O:CCM with sterile water and also incubated with the cells (Figure S4). Negative controls consisted of cells incubated with fresh CCM for 24 h and positive controls consisted of cells exposed to fresh CCM for 24 h followed by a 10 min incubation 100 µL of Triton-X 1% solution. Following incubation, cells were washed twice with 200 µL of warm PBS, then incubated for 4 h at 37°C with MTT solution (1 mg/mL [45]) followed by the addition of 100 µL of 10% SDS and 50% DMF solution [45] and incubation for 24 h at 37°C to solubilize the formazan crystals. Subsequently, the absorbance was measured at λ = 570 nm (formazan) in a plate reader (Spectramax 340 PC384). At 570 nm, the tested CPNs presented absorbance lower than 0.1 at 7 µg/mL PCPDTBT (conjugated polymer content in 150 µg/mL nanoparticle solution) and it was assumed that any residual CPN would not be at sufficient concentration to interfere with the formazan measurement. Cytotoxicity assays were repeated for a minimum of three times with different passage numbers, in accordance to the ISO 10993-5 (tests for *in vitro* cytotoxicity) [46]. To negate the effects of different sedimentation and diffusion velocities on the dose of nanoparticles reaching the cell layer, the cell viability results were plotted against the delivered dose (µg/cm^2) rather than the administered dose (µg/mL) [47]. The delivered dose values were calculated with the In Vitro Sedimentation, Diffusion and Dosimetry (ISDD) model [48], using the NTA-derived hydrodynamic diameters measured after 24 h in CCM as input values.

Haemocompatibility

The assessment of the nanoparticle interactions with relevant blood components involved the collection of blood from healthy volunteers, which provided consent, and the project was approved by the institutional Ethics Committee (reference 10/H0807/99).

Haemolysis: The haemolysis assay was based on a colorimetric detection of red-coloured cyanmethemoglobin (CMH) [49,33,50,51]. Duplicate samples of 100 µL of nanoparticle dispersions (300, 30, 3 µg/mL), water (the nanoparticle vehicle), DPBS (negative control) and Triton X-100 1% (positive control) were added to microcentrifuge tubes and incubated 3 h (± 15 min) at 37°C, with 100 µL of blood standardized to a haemoglobin concentration of 10 ± 2

mg/mL, with gentle mixing every 30 minutes. Samples were then centrifuged 15 minutes at 800 g and 100 µL supernatant was added to a 96-well plate containing 100 µL of CMH. The absorbance of the plate was read at 540 nm in a plate reader Spectramax 340 PC384 (Program Softmax pro 6.2.2) and haemoglobin concentrations were determined from a haemoglobin calibration curve. PCPDTBT content was accounted for by subtracting the background absorbance of samples containing nanoparticles, but no blood.

Platelet aggregation: The assessment of platelet aggregation was based light transmission aggregometry in a 96-well plate [52]. Briefly, platelet rich plasma (PRP) and platelet poor plasma (PPP) were isolated from whole human blood and 100 µL added to a 96 well plate. Nanoparticle dispersions were prepared in water so that when 10 µL were added to PRP/PPP samples a concentration of 300, 30, 3 µg/mL was achieved. Subsequently, samples were received either 10 µL ADP (12 mM in PBS) to induce platelet aggregation or 10 µL PBS only. Controls consisted of 100 µL PRP (0% aggregation) and 100 µL PRP containing 10 µL of ADP stock solution (100% aggregation), while PPP containing nanoparticles at different concentrations were used to subtract the background. To account for the plasma dilution by nanoparticle samples, 10 µL water was added to the controls and blank and PBS was used to complete the volume of samples to reach a standardized final volume of 120 µL. The transmittance was measured immediately following ADP addition at 595 nm (Spectramax 340 PC384). The analysis was performed at 37°C with a total read time of 16 minutes with interval measurements every 15 seconds and 7 seconds plate shaking before each read. In all the experiments, the number of platelets in PRP were within the normal range of 1.89-3.99x10^8 cells/mL [52].

Absorbance and emission spectra: Spectra of PCPDTBT dissolved in THF and nanoparticles diluted in water to 1.7 µg/mL PDPCTBT were measured with a wavelength-calibrated FluoroMax-4 spectrofluorometer (Horiba Jobin Yvon). The absorption spectra were acquired following 860 nm emission; emission spectra were acquired following 550 nm excitation. For both, absorption and emission spectra the excitation/emission slit was set to 1 nm and the integration time to 0.5 seconds.

Quantum yield: QY values were measured with the Fluoromax 4 using the PTI K-Sphere in the sample compartment. A 10 mm quartz cuvette was used. To avoid inner-filter effects from reabsorption, the sample was diluted that the absorbance at the excitation wavelength was less than 0.1. In order not to oversaturate the photomultiplier detector (PMT), the signal strength was checked in the real time control (RTC). Neutral-density filter (ND) were used on the excitation side to reduce the intensity on the Rayleigh scatter to stay within linear range of the detector (1 million to 1.5 million CPS on the raw S1 signal). Slits on the excitation and emission monochromators were set to 3 nm in the sample measurement. Integration time was set to 1 s. The area balance factor (ABF) needed for the QY tool was assessed by measuring the spectrum in question once with and without the required filter combination. The ABF is the quotient of the integrated curves of the relevant spectra.

Optical imaging performance in a phantom mouse: CPNs and Indocyanine green (ICG) were diluted in deionised water to give equivalent fluorophore masses of 0.125, 0.25. 0.5 and 1 µg per 10 µL. A further sample of ICG diluted in human serum albumin solution (40 mg/mL) was also prepared to mimic the effect of *in vivo* protein binding on ICG fluorescence [53,54]. A 10 µL volume of each sample was pipetted into a narrow silicon tube and positioned in one of two available bores in an XFM-2 phantom mouse (PerkinElmer/Caliper). The bores were located at 4.0 mm (ventral position) and 17.0 mm (dorsal position) distance from the imaging surface. Images were acquired using the epifluorescence mode of the IVIS Spectrum (PerkinElmer/Caliper). Samples within the mouse contained 0.125, 0.25, 0.5 and 1 µg fluorophore and images were acquired using the following excitation and emission wavelengths: λex= 745 nm, λem= 820 nm (ICG) and λex= 745 nm, λem= 840 nm (PCPDTBT). For all experiments an identical region of interest (ROI) was used to evaluation total radiant efficiency. From this, a signal-to-background ratio (SBR) was calculated for each wavelength combination using the phantom mouse without sample inside as a background reference. All quantitative measurements of fluorescence signal were performed utilizing the Living Image v. 4.3.1 software (PerkinElmer/Caliper).

PA imaging performance in a phantom: PA measurements were carried out by using the Vevo-LAZR X (FUJIFILM Visualsonics, The Netherlands). Vevo LAZR-X is a multimodal platform which allows the simultaneous imaging of high-resolution ultrasound and photoacoustics. The system was equipped with a linear array of ultrasound transducer at a central frequency 21 MHz (MX 250) and 2 fiber optic bundles on either side of the transducer for the illumination. The fiber bundle was coupled to a tunable Nd: YAG laser (680 to 970 nm) with a 20 Hz repetition rate. A commercially available phantom (Vevo Phantom, VisualSonics, Amsterdam) which consisted of transparent capillary tubes was used for the sample characterisation. The tubes were mounted on an acrylic dish filled with distilled water for better coupling of the generated sound signals. Different contrast agent masses (6.25-100 µg) were injected into the capillary tubing and the system acquired a sequence of PA images in the wavelength range of 680-970 nm with a step size of 5 nm in the spectral mode. After acquisition, images were analysed using Vevo LAB software (FUJIFILM Visualsonics, The Netherlands) and the spectral characteristics of the samples were recorded. 3-dimensional spectral imaging of the tubes was also performed using a 2D stepper-motor and linear translation of the transducer over the capillary tubes. Experiments were performed in triplicate.

Statistical analysis

The multivariate analysis of particle size determinants was performed with Excel 2013 (Microsoft, Inc). GraphPad Prism

(version 5.00 for Windows, GraphPad Software, San Diego California, USA) was used to perform all other statistical analyses (One-way ANOVA with Tukey post hoc test and regression analysis). Statistical significance values were described as * p≤0.05 ** p≤0.01, *** p≤0.001.

Results and discussion

Effect of PCPTDTBT content, total solids concentration and PEG-PLGA structure on CPN size

A multivariate analysis was performed to evaluate the effect of PCPDTBT content, total solids concentration and PEG-PLGA block composition (PEG_{2kDa}-$PLGA_{4kDa}$, PEG_{2kDa}-$PLGA_{15kDa}$ and PEG_{5kDa}-$PLGA_{55kDa}$) on the hydrodynamic diameters of CPNs. A minimum of eight formulations with varying PCPDTBT content (0-60%) and total solids concentration (0.1-2.4 mg/mL) were prepared for each PEG-PLGA grade and multivariate analysis was used to generate models predicting the influence of PCPDTBT content (x) and total solids concentration (y) on CPN hydrodynamic diameter (z; **Figure 2**). Regression analysis showed a moderate to good fit of the data (R^2=0.5600-0.9067) to the respective models generated for each of the three PEG-PLGA classes. The models indicated that systems composed of the two larger PEG-PLGA polymers, PEG_{2kDa}-$PLGA_{15kDa}$ and PEG_{5kDa}-$PLGA_{55kDa}$, were sensitive to changes in both the PCPDTBT content and total solids concentration, whereas the particle sizes of systems made from PEG_{2kDa}-$PLGA_{4kDa}$ were dependent only on PCPDTBT content. In general, both a reduction of the PCPDTBT content and total solids concentration led to a reduction in particle size with all three PEG-PLGA structures.

Despite the generally larger particle sizes obtained with 2.1 mg/mL total solids concentration, the higher particle concentration in these formulations facilitated subsequent characterisation and cytotoxicity studies and therefore this condition was carried forward combined with a low loading dose of 5% PCPDTBT. SEM micrographs of PEG_{2kDa}-$PLGA_{15kDa}$ and PEG_{5kDa}-$PLGA_{55kDa}$ systems prepared under these conditions (**Figure 3A/B**) showed spherical nanoparticles with median diameters smaller than 30 nm and a relatively high dispersity (**Figure 3C/D**). Although the hydrodynamic diameter of nanoparticles is typically larger than size measurements obtained under dry conditions [55,565], DLS data suggested a low polydispersity (<0.17), in contrast to the broad range of sizes shown by the SEM images.

The disparities in size in between the two techniques can be explained by the DLS measurements underestimating the detection of small nanoparticle populations, due to their lower light scattering. This observed DLS limitation has been previously reported [55,57]. Although the CPNs presented a broad size distribution, the observed size range was lower than previously described for PLGA nanoparticles (100-550 nm) also prepared by nanoprecipitation with PVA surfactant [58]. It is relevant to mention that most reports found in the literature used DLS to assess the size of PEG-PLGA nanoparticles and the majority of them did not show TEM or SEM images of nanoparticles produced [59–62] or did not estimate their size distribution from SEM/TEM images [11,63]. The results emphasize the importance of using multiple measurement techniques to characterise nanoparticle size and distribution.

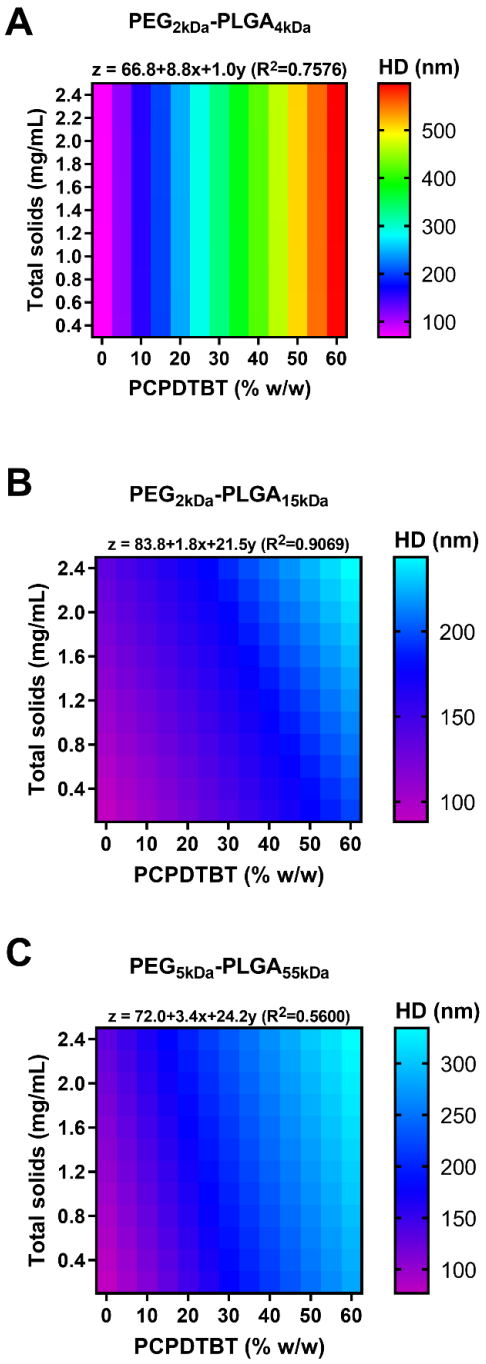

Figure 2: Effect of PCPDTBT content (% w/w; x) and total solids concentration (mg/mL; y) on nanoparticle hydrodynamic diameters (z) for systems produced from PEG_{2kDa}-$PLGA_{4kDa}$ (A), PEG_{2kDa}-$PLGA_{15kDa}$ (B), and PEG_{5kDa}-$PLGA_{55kDa}$ (C). Models were generated from the mean hydrodynamic diameters of n=3 different batches prepared under different processing conditions (8-14 variations per model).

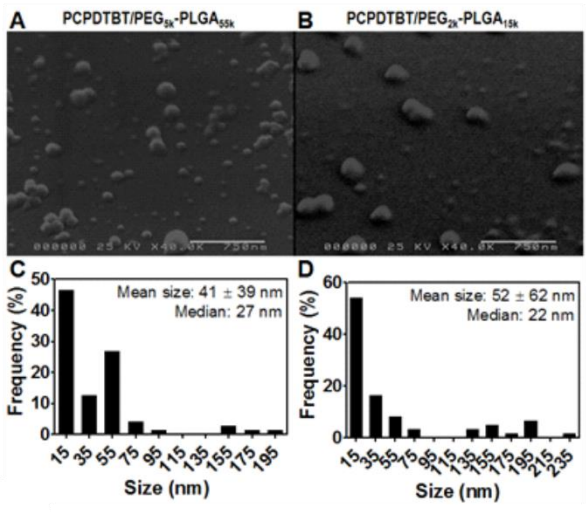

Figure 3: SEM micrographs of PEG_{5kDa}-$PLGA_{55kDa}$ (A) and PEG_{2kDa}-$PLGA_{15kDa}$ (B) CPNs containing 5% PCPDTBT (2.1 mg/mL total solids). The scale bar represents 750 nm. The size distributions of both systems were determined by ImageJ analysis (C and D, respectively).

Cytotoxicity

The MTT-based cytotoxicity technique is a rapid colorimetric assay broadly used for nanoparticle safety assessment [59]. According to ISO 10993-5, materials designed for biomedical applications that show cell viability above 80% are classified as having slight cytotoxicity, above 50% mild cytotoxicity and below 50% moderate toxicity, with the extremes of ~100% and ~0% being categorised as non-cytotoxic and severely cytotoxic, respectively [46]. Only the highest concentrations tested in this study reached values of 40-50% viability, i.e. moderate cytotoxicity, making the prediction of full dose-response curve slightly less reliable (R^2 values of curve fits ranged from 0.54-0.88) (**Figure 4**).

Nonetheless, differences between the systems were observed, for example, increasing PEG-PLGA molecular weight resulted in a greater cytotoxicity. Also, systems containing 5% PCPDTBT were marginally more cytotoxic than systems without the conjugated polymer. Since different hydrodynamic diameters were measured for each system, the ISDD model was used to calculate the delivered dose (μg/cm^2), i.e. the nanoparticle mass to reach the cell layer, taking sedimentation and diffusion behaviour of the particles into account [47,48]. This metric shows that differences in particle size are not responsible for the different cytotoxicity profiles seen here. Thus, it may be postulated that different PEG densities on the particle surface or perhaps different intracellular degradation kinetics may be responsible for the different cytotoxicity profiles. Both hypotheses are currently under investigation in a separate study.

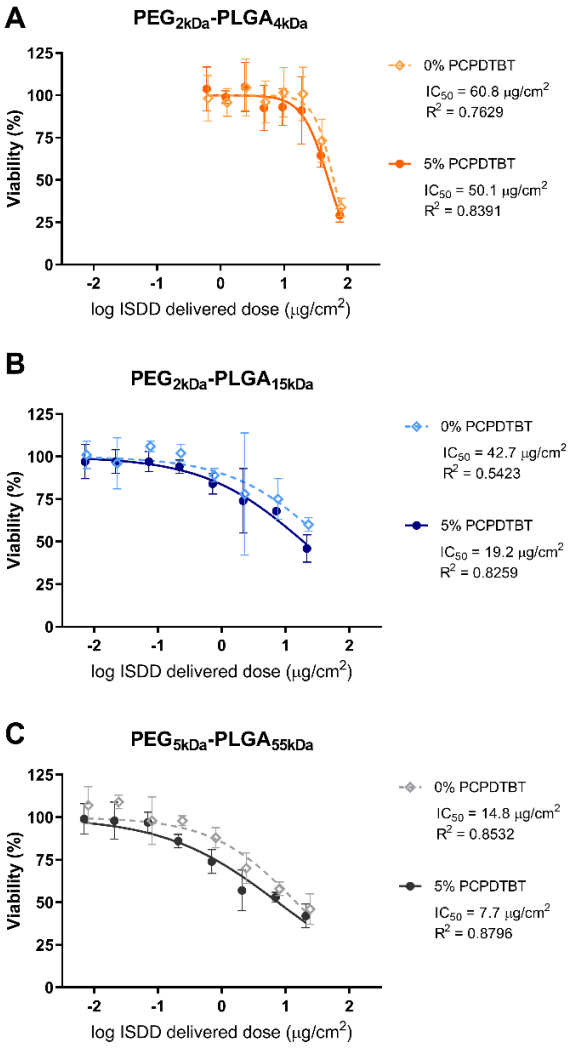

Figure 4: Comparison of the cytotoxicity of (A) PEG_{2kDa}-$PLGA_{4kDa}$, (B) PEG_{2kDa}-$PLGA_{15kDa}$ and C) PEG_{5kDa}-$PLGA_{55kDa}$ containing 0 and 5% PCPDTBT in a J774 macrophage-like *in vitro* model. Cell viability was plotted against the ISDD-calculated delivered dose (μg/cm^2) to negate the effects of different particle sizes on the sedimentation and diffusion behaviour of the particles. Values represent the mean ± standard deviation of n=3-6 experiments with different passage numbers.

Haemocompatitbility

The percent haemolysis induced by a test sample can be classified as non-haemolytic if lower than 2%, slightly haemolytic within 2-5% and haemolytic if higher than 5% [50,64,65]. Independent of the grade of PEG-PLGA and the presence of PCPDTBT, all nanoparticles were non-haemolytic at the concentrations tested, except for PEG_{2kDa}-$PLGA_{15kDa}$ containing 5% PCPDTBT, which presented a slight haemolytic activity (2.3 ± 1.5%) at 300 μg/mL (**Figure S2A, ESI**). As a comparison, CPNs coated with a pegylated phosphatidyl-ethanolamine ($PE\text{-}PEG_{2kDa}$) surface stabiliser had haemolysis values higher than 10-20% [33], indicating that excess free

or displaced surfactant is associated with higher than acceptable haemolysis values. Therefore, embedding conjugated polymers into PEG-PLGA nanoparticles is an advantageous formulation strategy to reduce haemolytic activity [33].

Nanoparticles intended for intravenous administration should ideally be inert to platelets to avoid both pronounced thrombosis and anti-thrombotic activity. For example, carbon-based nanoparticles have been reported to induce platelet aggregation and cause increased vascular thrombosis in rats [66]. In the current study, no induction of platelet aggregation was observed for all PEG-PLGA systems (**Figure S2B, ESI**). Neither did any system inhibit ADP-induced aggregation over a 16-minute test period (**Figure S2C, ESI**). This contrasts again with results reported by Khanbeigi, Hashim *et al* 2015 [33] who observed that PPE:PE-PEG_{2kDa} core-shell CPNs inhibited ADP-induced platelet aggregation in a dose-dependent manner. Surprisingly, similar CPNs containing PPV in the core did not show this effect [33].

Effect of PEG-PLGA structure on CPN optical and PA imaging performance

CPNs prepared with 5% PCPDTBT (2.1 mg/mL total solids) showed a slight blue shift in maximum absorbance compared to PCPDTBT dissolved in THF (~650 nm vs. ~690 nm, respectively), resulting from a decreased conjugation length due to the polymer bending in the particle core [67,68] (**Figure 5A**). The CPNs also exhibited a large red-shift in the emission spectra ($\lambda_{max.}$= 850 nm) in comparison to PCPDTBT in THF ($\lambda_{max.}$= 760 nm), caused by inter-chain species originating from increased chain interactions [35,38,56,67,69]. A red-shift similar magnitude has been previously reported for PCPDTBT nanoparticles coated with the phospholipid, DOPC, as compared to the conjugated polymer dissolved in chloroform [16]. Photoluminescence quantum yield values (PLQY%) of the CPNs were 30-100-fold lower than PCPDTBT in THF (**Figure 5B**). In spite of a similar red shift in their emission spectra, PLQY measurements of nanoparticles showed that the block copolymer influenced the optical properties of PCPDTBT, with CPNs of PEG_{2kDa}-$PLGA_{4kDa}$ presenting the highest PLQY.

An IVIS Spectrum optical imaging instrument (Perkin-Elmer) was employed to characterise the optical performance of the systems in a phantom mouse with similar autofluorescence and light scattering properties to murine muscle tissue [70]. Calculation of the signal to background ratios of the different fluorophores enabled comparisons between the PCPDTBT nanoparticles and the clinically approved NIR fluorophore, ICG (in water and an albumin solution representing serum), which has different excitation and emission characteristics (**Figure 6**). Despite the low quantum yield values of the CPNs compared to ICG, all three CPN systems showed a measurable signal:background ratio (SBR) in a phantom mouse model at concentrations > 250 ng, with a nearly linear increase in SBR up to 1 µg. As suggested by the slightly higher PLQY% value, the PEG_{2kDa}-$PLGA_{4kDa}$ (5% PCPDTBT) consistently outperformed the two other PEG-PLGA formulations.

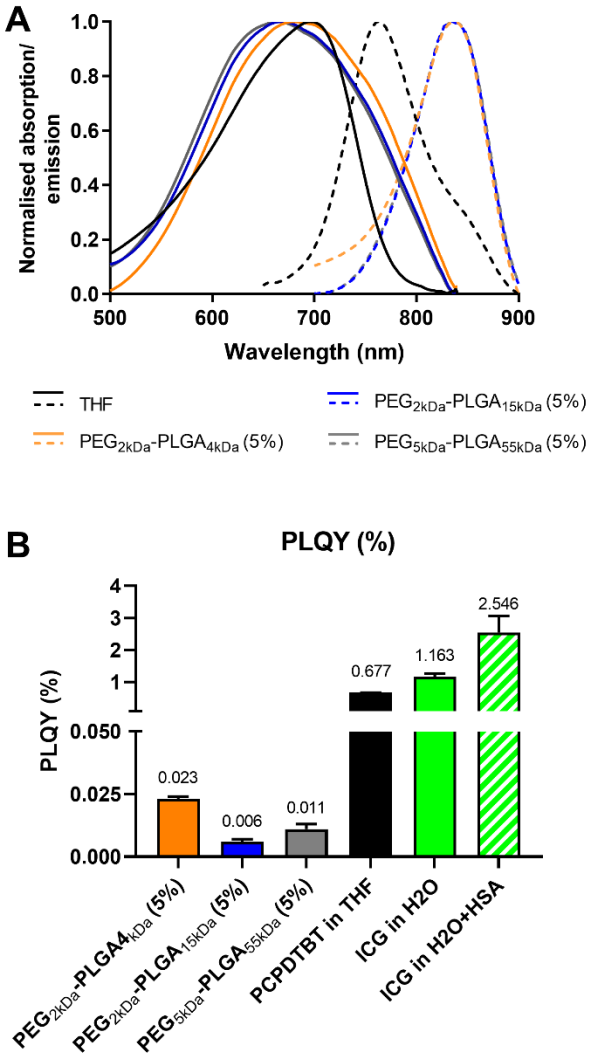

Figure 5: Normalised absorption and emission spectra of PCPDTBT in THF and 5% PCPDTBT:PEG-PLGA CPNs dispersed in water (A) and photoluminescence quantum yields of systems investigated (B). Values represented mean ± standard deviation of n=3 batches.

Resulting from a large molar extinction coefficient of approximately ε = $5x10^7$ $cm^{-1}M^{-1}$, strong thermalisation efficiency and consequently strong PA signal generation, PCPDTBT has primarily been investigated as a new contrast agent for PA imaging [10,11,15]. Consequently, it was of interest to assess whether the type of PEG-PLGA matrix polymer influenced the PA signal of PCPDTBT. Normalised PA amplitudes were measured at wavelengths ranging from 650 – 1000 nm with PCPDTBT systems showing a maximum at ~710 nm and ICG in water at ~825 nm (**Figure 7A**). Maximum PA amplitudes at increasing contrast agent masses (6.25-100 µg) were then determined in a phantom. The structure of PEG-PLGA had a noticeable influence on the maximal PA amplitude, with PEG_{2kDa}-$PLGA_{4kDa}$ systems showing a much steeper increase in signal with increasing dose compared with the other two PEG-PLGA systems

(**Figure 7B**). At the highest mass, the PA amplitude decreased for PEG_{2kDa}-$PLGA_{4kDa}$, to levels comparable to the other two systems. It should be noted that the signal variability also increased substantially at 100 µg, indicating that the results from this amount of contrast agent were less reliable. In comparison to PCPDTBT, the ICG sample in water increased exponentially from 6.25-25 µg above which, the PA amplitude remained the same.

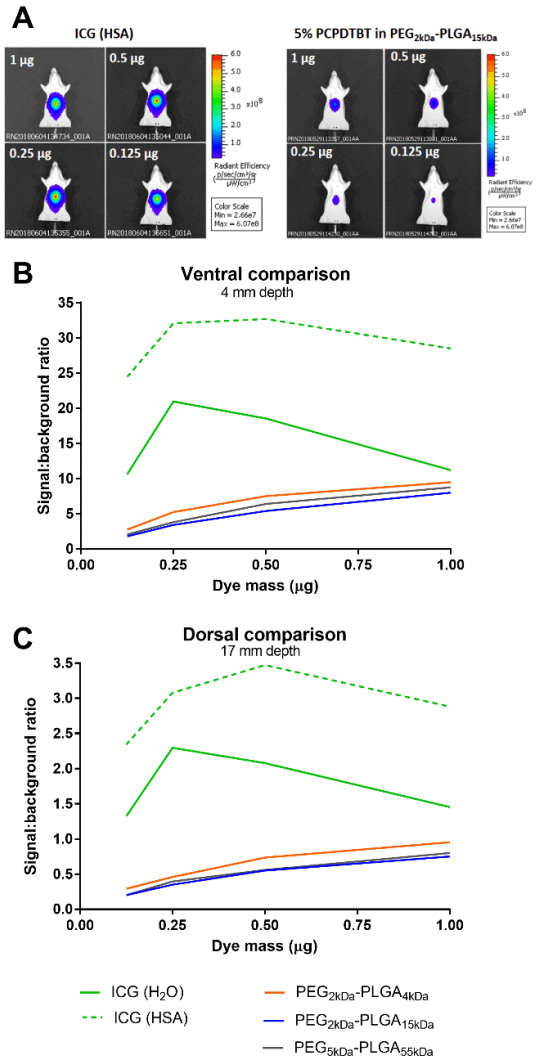

Figure 6: Optical performance of 5% PCPDTBT in three different PEG-PLGA nanoparticle systems in a phantom mouse. A) Representative images of the control, 0.125 – 1 µg ICG in a human serum albumin solution (40 mg/mL), compared with 0.125 – 1 µg PCPDTBT encapsulated in PEG_{2kDa}-$PLGA_{15kDa}$. SBR ratios for dye mass values of 0.125, 0.25, 0.5 and 1 µg were calculated from whole body imaging of a phantom mouse from the B) ventral (4 mm penetration depth) and C) dorsal (17 mm penetration depth) sides. Values depicted are from a single nanoparticle batch.

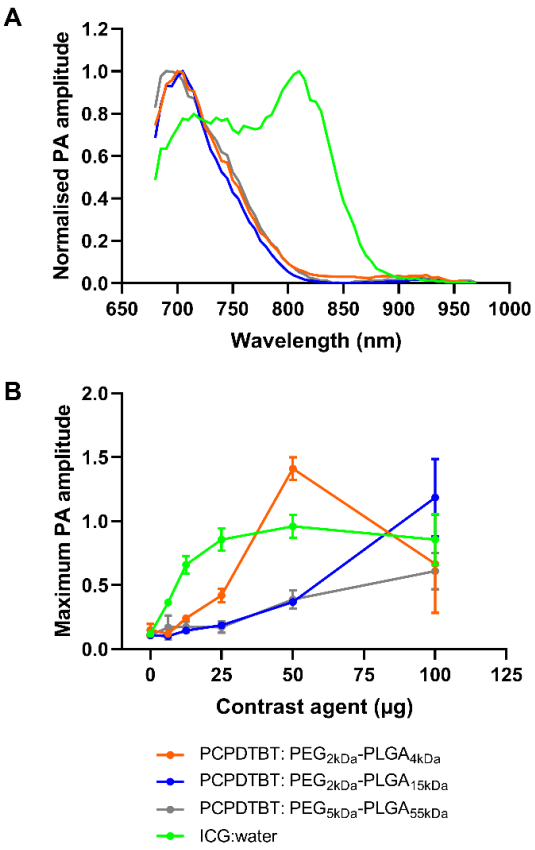

Figure 7: Normalised PA amplitude spectra (A) and dose-dependency of maximal PA amplitude values (B) of 5% PCPDTBT:PEG-PLGA CPNs dispersed in water compared with an aqueous ICG solution. Values represent the mean ± SD of n=3 experiments from a single batch.

To our knowledge, this study represents the first report of a nanoparticle matrix material influencing the optical and PA performance of a conjugated polymer. Throughout the study, the PEG_{2kDa}-$PLGA_{4kDa}$ CPNs showed a slight, but consistently better performance with regard to physicochemical properties, biocompatibility, optical and PA imaging performance than the higher molar mass analogues. The reasons for this are not fully clear, although it may be postulated that the low molecular weight, more hydrophilic PEG_{2kDa}-$PLGA_{4kDa}$ is able to diffuse more rapidly into the aqueous medium during the nanoprecipitation event leading to formation of a nanoparticle core enriched in PCPDTBT and coated with a layer of PEG_{2kDa}-$PLGA_{4kDa}$ at the particle surface. In contrast, the larger, more slowly diffusing PEG-PLGA analogues may show a higher degree of co-precipitation in the nanoparticle core. The presence of PEG-PLGA in the nanoparticle core might enable a higher degree of water penetration into the core [75] as compared to a putative PCPDTBT-enriched core structure. Water penetration in the nanoparticle core could result in the larger hydrodynamic diameters, photoluminescence quenching without a shift in the emission maximum, as well as changes in conversion efficiency from light absorption to ultrasound emission leading to reduced PA amplitudes again without an accompanying shift in the PA amplitude spectrum,

all effects which were observed in this study. Techniques such as small angle neutron scattering would be suitable to investigate this hypothesis and could be the focus of future studies.

Conclusions

The self-assembling diblock copolymer, PEG-PLGA, has been shown to improve CPN characteristics, irrespective of conjugated polymer chemistry [25,26]. The advantages of PEG-PLGA as a matrix forming agent for conjugated polymer encapsulation include small particle sizes, circumvention of the use of adsorbed surfactant to ensure colloidal stability and thus no surfactant-related toxicity. PEG-PLGA CPN systems show excellent stability in biofluids, a high cytocompatibility, excellent haemocompatibility, and promising optical performance. To date, the impact of PEG-PLGA structure on CPN properties had not been assessed. The current study demonstrated that the use of a PEG-PLGA with a relative short PLGA block (i.e. $PLGA_{4kDa}$) with a 2 kDa PEG group conferred benefits compared to PEG-PLGAs with longer PLGA chains. Overall, the. PEG_{2kDa}-$PLGA_{4kDa}$ systems were smaller in size, had a reduced cytotoxicity and a slightly enhanced optical performance compared to CPNs produced with PEG_{2kDa}-$PLGA_{15kDa}$ and PEG_{5kDa}-$PLGA_{55kDa}$.

Conflicts of interest

There are no conflicts to declare.

Acknowledgements

The Brazilian agency *Coordenação de Aperfeiçoamento de Pessoal de Nível Superior* (CAPES) and the programme Science Without Borders for the full 4-year PhD scholarship and funding provided (process number 0685/13-5). Dr Simon Pitchford for his help with the haemocompatibility assays. This work was supported by the Engineering and Physical Sciences Research Council [Grant Numbers EP/K018876/1, EP/N03371X/1].

Notes and references

1 G. Hibbs, *Nat. Mater.*, 2014, **13**, 99–99.
2 R. Tang and X. Feng, *Can. Chem. Trans.*, 2013, **1**, 78–84.
3 D. Tuncel and H. V. Demir, *Nanoscale*, 2010, **2**, 484–494.
4 K. Colladet, M. Nicolas, L. Goris, L. Lutsen and D. Vanderzande, *Thin Solid Films*, 2004, **451**–**452**, 7–11.
5 D. Mühlbacher, M. Scharber, M. Morana, Z. Zhu, D. Waller, R. Gaudiana and C. Brabec, *Adv. Mater.*, 2006, **18**, 2884–2889.
6 G. L. Schulz, F. S. U. Fischer, D. Trefz, A. Melnyk, A. Hamidi-Sakr, M. Brinkmann, D. Andrienko and S. Ludwigs, *Macromolecules*, 2017, **50**, 1402–1414.
7 J. Hou, *J. Am. Chem. Soc.*, 2008, **130**, 16144–16145.
8 S.-W. Chang, J. Kettle, H. Waters and M. Horie, *RSC Adv.*, 2015, **5**, 107276–107284.
9 S.-W. Chang, T. Muto, T. Kondo, M.-J. Liao and M. Horie, *Polym. J.*, 2017, **49**, 113–122.
10 K. Pu, A. J. Shuhendler, J. V. Jokerst, J. Mei, S. S. Gambhir, Z. Bao and J. Rao, *Nat. Nanotechnol.*, 2014, **9**, 233–9.
11 Y. Lyu, Y. Fang, Q. Miao, X. Zhen, D. Ding and K. Pu, *ACS Nano*, 2016, **10**, 4472–4481.
12 D. Zhang, M. Wu, Y. Zeng, N. Liao, Z. Cai, G. Liu, X. Liu and J. Liu, *J. Mater. Chem. B*, 2016, **4**, 589–599.
13 Y. Lyu, X. Zhen, Y. Miao and K. Pu, *ACS Nano*, 2017, **11**, 358–367.
14 H. Zhu, Y. Fang, X. Zhen, N. Wei, Y. Gao, K. Q. Luo, C. Xu, H. Duan, D. Ding, P. Chen and K. Pu, *Chem. Sci.*, 2016, **7**, 5118–5125.
15 X. Qin, H. Chen, H. Yang, H. Wu, X. Zhao, H. Wang, T. Chour, E. Neofytou, D. Ding, H. Daldrup-Link, S. C. Heilshorn, K. Li and J. C. Wu, *Adv. Funct. Mater.*, 2018, **28**, 1–12.
16 J. Yoon, J. Kwag, T. J. Shin, J. J. Park, Y. M. Y. Lee, Y. M. Y. Lee, J. J. Park, J. Heo, C. Joo, T. J. Park, P. J. Yoo and S. Kim, *Adv. Mater.*, 2014, **26**, 4559–4564.
17 C. M. Macneill, R. C. Coffin, D. L. Carroll and N. H. Levi-Polyachenko, *Macromol. Biosci.*, 2013, **13**, 28–34.
18 H. Zhu, J. Li, X. Qi, P. Chen and K. Pu, *Nano Lett.*, 2018, **18**, 586–594.
19 Y. K. Choi, D. Lee, S. Y. Lee, T. J. Shin, J. Park and D. J. Ahn, *Macromolecules*, 2017, acs.macromol.7b01367.
20 T. Stahl, R. Bofinger, I. Lam, K. J. Fallon, P. Johnson, O. Ogunlade, V. Vassileva, R. B. Pedley, P. C. Beard, H. C. Hailes, H. Bronstein and A. B. Tabor, *Bioconjug. Chem.*, 2017, **28**, 1734–1740.
21 X. Zhen, X. Feng, C. Xie, Y. Zheng and K. Pu, *Biomaterials*, 2017, **127**, 97–106.
22 R. A. Khanbeigi, T. F. Abelha, A. Woods, O. Rastoin, R. D. Harvey, M.-C. Jones, B. Forbes, M. A. Green, H. Collins and L. A. Dailey, *Biomacromolecules*, 2015, **16**, 733–742.
23 J. M. Chan, P. M. Valencia, L. Zhang, R. Langer and O. C. Farokhzad, in *Methods in Molecular Biology*, eds. S. R. Grobmyer and B. M. Moudgil, Humana Press, Totowa, NJ, 2010, vol. 624, pp. 163–175.
24 K. Zhang, X. Tang, J. Zhang, W. Lu, X. Lin, Y. Zhang, B. Tian, H. Yang and H. He, *J. Control. release*, 2014, **183**, 77–86.
25 T. F. Abelha, T. W. Phillips, J. H. Bannock, A. M. Nightingale, C. A. Dreiss, E. Kemal, L. Urbano, J. C. de Mello, M. A. Green and L. A. Dailey, *Nanoscale*, 2017, **9**, 2009–2019.
26 E. Kemal, T. F. Abelha, L. Urbano, R. Peters, D. M. Owen, P. Howes, M. Green and L. A. Dailey, *RSC Adv.*, 2017, **7**, 15255–15264.
27 B. Romberg, W. E. Hennink and G. Storm, *Pharm. Res.*, 2008, **25**, 55–71.
28 S. Schubert, J. T. Delaney, Jr and U. S. Schubert, *Soft Matter*, 2011, **7**, 1581–1588.
29 P. M. Valencia, O. C. Farokhzad, R. Karnik and R. Langer,

Nat. Nanotechnol., 2012, **7**, 623–9.
30 S. Naahidi, M. Jafari, F. Edalat, K. Raymond, A. Khademhosseini and P. Chen, *J. Control. Release*, 2013, **166**, 182–194.
31 M. A. Dobrovolskaia, S. E. McNeil and S. E. M. Neil, *Nat. Nanotechnol.*, 2007, **2**, 469–78.
32 K. Li, J. Pan, S. S. Feng, A. W. Wu, K. Y. Pu, Y. Liu and B. Liu, *Adv. Funct. Mater.*, 2009, **19**, 3535–3542.
33 R. A. Khanbeigi, Z. Hashim, T. F. Abelha, S. Pitchford, H. Collins, M. Green and L. A. Dailey, *J. Mater. Chem. B*, 2015, **3**, 2463–2471.
34 G. Hong, Y. Zou, A. L. Antaris, S. Diao, D. Wu, K. Cheng, X. Zhang, C. Chen, B. Liu, Y. He, J. Z. Wu, J. Yuan, B. Zhang, Z. Tao, C. Fukunaga and H. Dai, *Nat. Commun.*, 2014, **5**, 1–9.
35 C. Wu, B. Bull, C. Szymanski, K. Christensen and J. McNeill, *ACS Nano*, 2008, **2**, 2415–2423.
36 Y.-H. Chan, F. Ye, M. E. Gallina, X. Zhang, Y. Jin, I.-C. Wu and D. T. Chiu, *J. Am. Chem. Soc.*, 2012, **134**, 7309–12.
37 P. K. Kandel, L. P. Fernando, P. C. Ackroyd and K. A. Christensen, *Nanoscale*, 2011, **3**, 1037–1045.
38 K. Sun, H. Chen, L. Wang, S. Yin, H. Wang, G. Xu, D. Chen, X. Zhang, C. Wu and W. Qin, *ACS Appl. Mater. Interfaces*, 2014, **6**, 10802–10812.
39 S. Kim, C.-K. Lim, J. Na, Y.-D. Lee, K. Kim, K. Choi, J. F. Leary and I. C. Kwon, *Chem. Commun.*, 2010, **46**, 1617–1619.
40 R. Dhankar, P. Rathee, A. K. Jain, S. Arora, S. Kumar, G. Rath, A. K. Saxena, P. R. Sharma and A. K. Goyal, *J. Appl. Pharm. Sci.*, 2011, **01**, 132–139.
41 R. Gref, M. Luck, P. Quellec, M. Marchand, E. Dellacherie, S. Harnisch, T. Blunk and R. H. Mullller, *Colloids Surfaces B Biointerfaces 18*, 2000, **18**, 301–313.
42 C. A. Schneider, W. S. Rasband and K. W. Eliceiri, *Nat. Methods*, 2012, **9**, 671–675.
43 T. R. Chen, *TCA Man. / Tissue Cult. Assoc.*, 1975, **1**, 229–232.
44 E. Hoffman, A. Kumar, V. Kanabar, M. Arno, L. Preux, V. Millar, C. Page, H. Collins, I. Mudway, L. A. Dailey and B. Forbes, *Mol. Pharm.*, 2015, **12**, 2675–2687.
45 M. B. Hansen, S. E. Nielsen and K. Berg, *J. Immunol. Methods*, 1989, **119**, 203–210.
46 ISO 10993-5, in *Biological Evaluation of Medical Devices*, International Organization for Standardization, Geneva, Switzerland., 3rd edn., 2009.
47 R. A. Khanbeigi, A. Kumar, F. Sadouki, C. Lorenz, B. Forbes, L. A. Dailey and H. Collins, *J. Control. release*, 2012, **162**, 259–66.
48 P. M. Hinderliter, K. R. Minard, G. Orr, W. B. Chrisler, B. D. Thrall, J. G. Pounds and J. G. Teeguarden, *Part. Fibre Toxicol.*, 2010, **7**, 36.
49 W. C. Stadie, *J. Biol. Chem.*, 1920, **41**, 237–241.
50 ASTM E2524-08, *Standard Test Method for Analysis of Hemolytic Properties of Nanoparticles*, 2013.
51 M. a Dobrovolskaia, J. D. Clogston, B. W. Neun, J. B. Hall, K. Anil and S. E. Mcneil, *Nano Lett.*, 2009, **8**, 2180–2187.
52 P. C. J. Armstrong, A. R. Dhanji, N. J. Truss, Z. N. M. Zain, A. T. Tucker, J. A. Mitchell and T. D. Warner, *Thromb. Haemost.*, 2009, **102**, 772–778.
53 R. Philip, A. Penzkofer, W. Biiumler, R. M. Szeimies and C. Abels, 1996, **96**, 137–148.
54 J. T. Alander, I. Kaartinen, A. Laakso, P. Tommi, T. Spillmann, V. V Tuchin, M. Venermo and V. Petri, , DOI:10.1155/2012/940585.
55 H. Fissan, S. Ristig, H. Kaminski, C. Asbach and M. Epple, *Anal. Methods*, 2014, **6**, 7324–7334.
56 P. K. Kandel, L. P. Fernando, P. C. Ackroyd and K. A. Christensen, *Nanoscale*, 2011, **3**, 1037–1045.
57 Y. Dieckmann, H. Cölfen, H. Hofmann and A. Petri-Fink, *Anal. Chem.*, 2009, **81**, 3889–3895.
58 H. Xie and J. W. Smith, *J. Nanobiotechnology*, 2010, **8**, 1–7.
59 J.-M. Lim, N. Bertrand, P. M. Valencia, M. Rhee, R. Langer, S. Jon, O. C. Farokhzad and R. Karnik, *Nanomedicine*, 2014, **10**, 401–9.
60 R. Karnik, F. Gu, P. Basto, C. Cannizzaro, L. Dean, W. Kyei-Manu, R. Langer and O. C. Farokhzad, *Nano Lett.*, 2008, **8**, 2906–12.
61 P. M. Valencia, P. A. Basto, L. Zhang, M. Rhee, R. Langer, O. C. Farokhzad and R. Karnik, *ACS Nano*, 2010, **4**, 1671–1679.
62 X. Kang, C. Luo, Q. Wei, C. Xiong, Q. Chen, Y. Chen and Q. Ouyang, *Microfluid. Nanofluidics*, 2013, **15**, 337–345.
63 Y. Haggag, Y. Abdel-Wahab, O. Ojo, M. Osman, S. El-Gizawy, M. El-Tanani, A. Faheem and P. McCarron, *Int. J. Pharm.*, 2016, **499**, 236–246.
64 F. Schlenk, S. Werner, M. Rabel, F. Jacobs, C. Bergemann, J. H. Clement and D. Fischer, *Arch. Toxicol.*, 2017, **10**, 3271–3286.
65 ASTM F 756-00, *Standard practice for assessment of hemolytic properties of materials.*, 2000.
66 A. Radomski, P. Jurasz, D. Alonso-Escolano, M. Drews, M. Morandi, T. Malinski and M. W. Radomski, *Br. J. Pharmacol.*, 2005, **146**, 882–93.
67 C. Wu, C. Szymanski and J. McNeill, *Langmuir*, 2006, **22**, 2956–60.
68 G. Padmanaban and S. Ramakrishnan, *J. Am. Chem. Soc.*, 2000, **122**, 2244–2251.
69 G. Padmanaban and S. Ramakrishnan, *J. Phys. Chem. B*, 2004, **108**, 14933–14941.
70 D. L. Crossley, L. Urbano, R. Neumann, S. Bourke, J. Jones, L. A. Dailey, M. Green, M. J. Humphries, S. M. King, M. L. Turner and M. J. Ingleson, *ACS Appl. Mater. Interfaces*, 2017, **9**, 28243–28249.